

Extragalactic Distances from Planetary Nebulae

Robin Ciardullo

The Pennsylvania State University, Department of Astronomy and Astrophysics, 525 Davey Lab University Park, PA 16803, USA

Abstract. The [O III] $\lambda 5007$ planetary nebula luminosity function (PNLF) occupies an important place on the extragalactic distance ladder. Since it is the only method that is applicable to all the large galaxies of the Local Supercluster, it is uniquely useful for cross-checking results and linking the Population I and Population II distance scales. We review the physics underlying the method, demonstrate its precision, and illustrate its value by comparing its distances to distances obtained from Cepheids and the Surface Brightness Fluctuation (SBF) method. We use the Cepheid and PNLF distances to 13 galaxies to show that the metallicity dependence of the PNLF cutoff is in excellent agreement with that predicted from theory, and that no additional systematic corrections are needed for either method. However, when we compare the Cepheid-calibrated PNLF distance scale with the Cepheid-calibrated SBF distance scale, we find a significant offset: although the relative distances of both methods are in excellent agreement, the PNLF method produces results that are systematically shorter by $\sim 15\%$. We trace this discrepancy back to the calibration galaxies and show how a small amount of internal reddening can lead to a very large systematic error. Finally, we demonstrate how the PNLF and Cepheid distances to NGC 4258 argue for a short distance to the Large Magellanic Cloud, and a Hubble Constant that is $\sim 8\%$ larger than that derived by the *HST* Key Project.

1 Introduction

The brightest stars have been used as extragalactic distance indicators ever since the days of Edwin Hubble [1]. However, it was not until the early 1960's that it was appreciated that young planetary nebulae (PNe) also fall into the "brightest stars" category. In their early stages of evolution, planetary nebulae are just as luminous as their asymptotic giant branch (AGB) progenitors; the fact that most of their continuum emission emerges in the far ultraviolet, instead of the optical or near infrared, in no way affects their detectability. On the contrary, because most of the central star's flux comes out at energies shortward of 13.6 eV, the physics of photoionization guarantees that this energy is reprocessed into a series of optical, IR, and near-UV emission lines. In fact, $\sim 10\%$ of the flux emitted by a young, planetary nebula comes out in a single emission line of doubly-ionized oxygen at 5007 Å. Thus, for cosmological purposes, a PN can be thought of as a cosmic apparatus which transforms continuum emission into monochromatic flux.

Although the idea of using PNe as standard candles was first presented in the early 1960's [2,3], it was not until the late 1970's that pioneering efforts in the

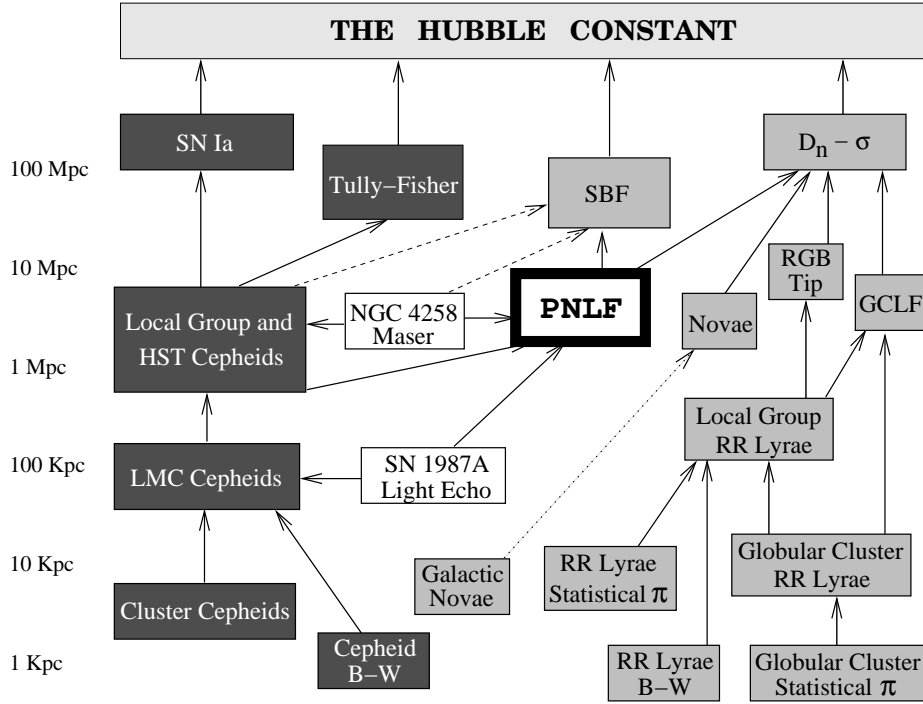


Fig. 1. The extragalactic distance ladder. The dark boxes show techniques useful in star-forming galaxies, the lightly-filled boxes give methods that work in Pop II systems, and the open boxes represent geometric distance determinations. Uncertain calibrations are noted as dashed lines. The PNLF is the only method that is equally effective in all the populations of the Local Supercluster.

field were made. Ford and Jenner [4] had noticed that the visual magnitudes of the brightest planetary nebulae in M31, M32, NGC 185, and NGC 205 were the same to within ~ 0.5 mag. This suggested that bright planetary nebulae could be used as standard candles. Based on this premise, crude PN-based distances were obtained to M81 [4], NGC 300 [5], and even several Local Group dwarfs [6]. These distance estimates were not very persuasive, since at the time nothing was known about the systematics of bright planetary nebulae or their luminosity function. Moreover, it had long been known that Galactic PNe are definitely *not* standard candles [7,8,9]. (It is an irony of the subject that in the Milky Way, factor of two distance errors are the norm [10,11,12,13,14].) Thus, it was not until 1989 when the [O III] $\lambda 5007$ PN luminosity function (PNLF) was modeled [15], and compared to the observed PNLFs of M31 [16], M81 [17], and the Leo I Group [18], that PNe became generally accepted as a distance indicator. Today, the [O III] $\lambda 5007$ PNLF is one of the most important standard candles in extragalactic astronomy, and the only method that can be applied to all the large galaxies of the Local Supercluster, regardless of environment or Hubble type (see Fig. 1).

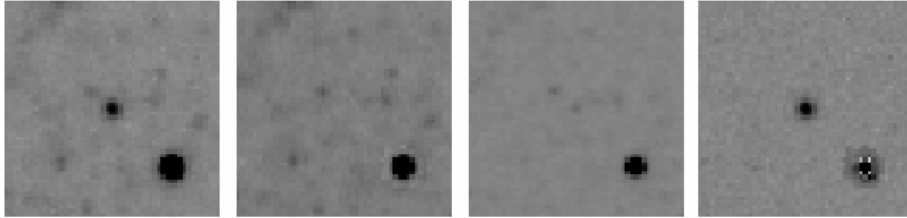


Fig. 2. The first three panels show images of a PN in NGC 2403 in [O III] $\lambda 5007$, continuum $\lambda 5300$, and $H\alpha$. The last column displays the [O III] on-band minus off-band difference image. The PN candidate is in the middle of the frame. All PNe in the top ~ 1 mag of the PNLF are stellar, invisible in the continuum, and much brighter in [O III] $\lambda 5007$ than $H\alpha$.

2 Planetary Nebula Identifications

PNLF observations begin with the selection of a narrow-band filter. Ideally, this filter should be centered at 5007 Å at the redshift of the target galaxy and be 25 Å to 50 Å wide. Narrower filters may miss objects that are redshifted out of the filter’s bandpass by the galaxy’s internal velocity dispersion, while broader filters admit too much continuum light and invite contamination by [O III] $\lambda 4959$. One subtlety of the process is that the characteristics of the filter at the telescope will not be the same as those in the laboratory. The central wavelength of an interference filter typically shifts ~ 0.2 Å to the blue for every 1° C drop in temperature. In addition, fast telescope optics will lower the filter’s peak transmission, shift its central wavelength to the blue, and drastically broaden its bandpass [19]. The observer must consider these factors when planning an observation, since without an accurate knowledge of the filter transmission curve, precise PN photometry is not possible.

PN observations in early-type galaxies are extremely simple. One images the galaxy through the narrow on-band filter, and then takes a similar image through a broader, off-band filter. The two frames are then compared, either by “blinking” the on-band image against the off-band image, or by creating an on-band minus off-band “difference” frame. Point sources which appear on the on-band frame, but are completely invisible on the offband frame, are planetary nebula candidates (see Fig. 2). In this era of wide-field mosaic CCD cameras, V filters are often used in place of true off-band filters. This works for most extragalactic programs, but is not ideal. Since the V -band includes the 5007 Å emission line, its use as an “off-band” may cause bright PNe to appear (faintly) in the continuum. Photometric techniques which use the difference image will therefore be compromised.

Since virtually every [O III] $\lambda 5007$ source in an elliptical or lenticular galaxy is a planetary nebula, PNLF measurements in these systems are straightforward. However, in spiral and irregular galaxies, this is not the case. H II regions and supernova remnants are also strong [O III] $\lambda 5007$ emitters, and in late-type

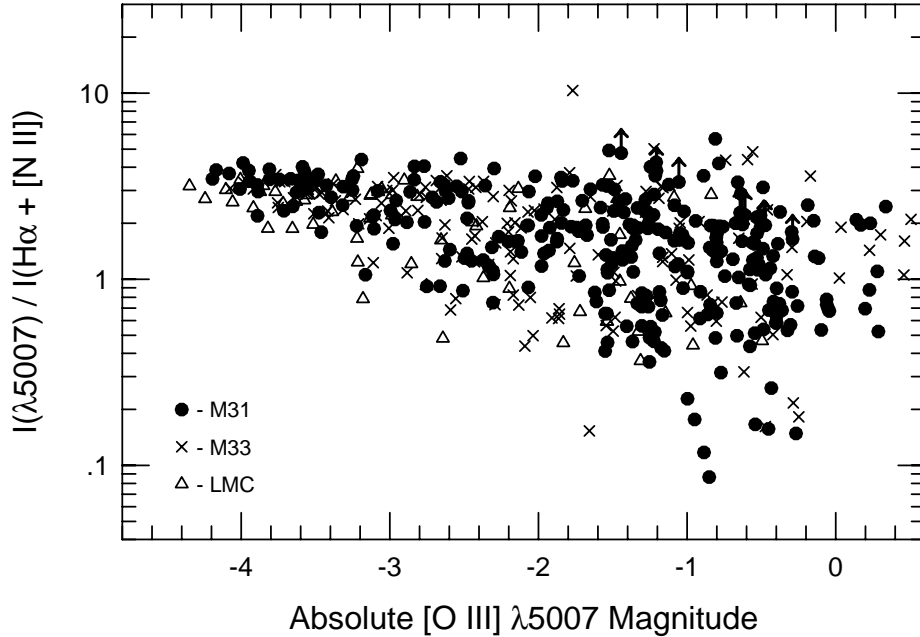


Fig. 3. The [O III] $\lambda 5007$ to $H\alpha + [N II]$ line ratio for PNe in the bulge of M31 [16], the disk of M33 [22], and the Large Magellanic Cloud [23,24,25,26]. This line ratio is useful for discriminating bright PNe from compact H II regions.

systems, these objects can numerically overwhelm the planetaries. Fortunately, most H II regions are resolvable (at least in galaxies closer than ~ 10 Mpc), whereas extragalactic PNe, which are always less than 1 pc in radius [20], are stellar. Thus, any object that is not a point source can immediately be eliminated from the sample. To remove the remaining contaminants, one can use $H\alpha$ as a discriminant. Planetary nebulae inhabit a distinctive region of [O III] $\lambda 5007$ - $H\alpha$ emission-line space. As illustrated in Fig. 3, objects in the top magnitude of the PNLF all have $\lambda 5007$ to $H\alpha + [N II]$ line ratios greater than ~ 2 . This is in contrast to H II regions, which typically have ratios less than one [21]. This difference in excitation is an effective diagnostic for removing whatever compact H II regions remain in the sample.

There are two other sources of contamination which may occur in deep planetary nebula surveys. The first is background galaxies. At $z = 3.12$, $Ly\alpha$ is redshifted in the bandpass of the [O III] $\lambda 5007$ filter, and at fluxes below $\sim 10^{-16}$ ergs cm^{-2} s^{-1} , unresolved and marginally resolved galaxies with extremely strong $Ly\alpha$ emission (equivalent widths $\gtrsim 300$ Å in the observers frame) do exist [27,28,29]. Fortunately, the density of these extraordinary objects is relatively low, ~ 1 arcmin $^{-2}$ per unit redshift interval brighter than 5×10^{-17} ergs cm^{-2} s^{-1} [30]. Thus while an occasional high-redshift interloper

may be found within the body of a galaxy [31], these objects are unlikely to distort the shape of the luminosity function.

The second source of confusion is specific to the Virgo Cluster. Between 10% and 20% of the stellar mass of rich clusters lies outside of any galaxy in intergalactic space [32,33,34]. PN surveys within these systems will therefore be contaminated by intracluster objects. In clusters such as Fornax, where the line-of-sight thickness is small [35,36], the effect of intracluster planetaries on the target galaxy’s PNLF is minimal. However, the Virgo Cluster’s depth is substantial [37,38,39,40], so surveys in this direction will contain a significant number of foreground sources. These intracluster objects can distort the galactic PNLF and possibly produce a biased distance estimate. The best way to minimize the effect is to limit PN surveys to the inner regions of galaxies (where the ratio of galactic to intracluster light is high), or statistically subtract the contribution of intracluster objects [41].

3 Deriving Distances

Once the PNe are found, the next step is to measure their brightnesses and define a statistically complete sample. The first step is easy. A significant advantage of the PNLF method is that it does not require complex crowded-field photometric algorithms. Raw instrumental magnitudes can be derived using simple aperture photometry or point-spread-function fitting procedures, and then turned into monochromatic [O III] $\lambda 5007$ fluxes using the techniques described in [42]. These fluxes are usually quoted in terms of magnitudes via

$$m_{5007} = -2.5 \log F_{5007} - 13.74 \quad (1)$$

The zero point of this system is not completely arbitrary. In this “standard” system, a PN’s $\lambda 5007$ magnitude is roughly equal to the magnitude it would have if viewed through the broadband V filter [15]. Bright PNe in M31 have $m_{5007} \sim 20$, while the brightest planetaries in Virgo have $m_{5007} \sim 26.5$.

The determination of statistically complete samples can be more time consuming. Although the onset of incompleteness can be found via the “traditional” method of adding artificial stars to frames and measuring the recovery fraction, there is a short cut. Experiments have shown that PN counts are not affected by incompleteness until the recorded signal-to-noise drops below a threshold value of ~ 10 [43,44]. Since extragalactic PNe are faint, this means that the probability of PN detection is a function of two parameters: the instrumental magnitude of the planetary, and the brightness of the underlying background. In early-type systems, where the galactic background is smooth and well-behaved, the creation of a statistical sample is therefore straightforward. One chooses an isophote and uses the signal-to-noise threshold to calculate the completeness limit (see [17,18]). In spiral and irregular galaxies, where the underlying background is irregular and complex, the process is more empirical: one selects the brightest (most uncertain) background in the sample, and uses the signal-to-noise each PN would have if it were projected on that background [45]. In

either case, the limiting magnitude for completeness need not be precise. The PNLF method depends far more on the brightest objects in the sample than the dimmest; small errors at the faint end of the luminosity function have little effect on the final derived distance.

Once a statistical sample of planetaries has been defined, PNLF distances are obtained by fitting the observed luminosity function to an empirical law. For simplicity, Ciardullo *et al.* [16] have fit the bright-end cutoff with the function

$$N(M) \propto e^{0.307M} \{1 - e^{3(M^* - M)}\} \quad (2)$$

though other forms of the relation are possible [46]. In the above equation, the key parameter is M^* , the absolute magnitude of the brightest possible planetary nebula. Despite some efforts at Galactic calibrations [47,46], the PNLF remains a secondary standard candle. The original value for the zero point, $M^* = -4.48$, was based on an M31 infrared Cepheid distance of 710 kpc [48] and a foreground extinction of $E(B - V) = 0.11$ [49]. Since then, M31's distance has increased [50], its reddening has decreased [51], and, most importantly, the Cepheid distances to 12 additional galaxies have been included in the calibration [52]. Somewhat fortuitously, the current value of M^* is only 0.01 mag fainter than the original value, $M^* = -4.47$ [52].

Before proceeding further, it is important to note that equation (2) only seeks to model the top ~ 1 mag of the PN luminosity function. At fainter magnitudes, large population-dependent differences exist. For example, in M31's bulge the PNLF monotonically increases according to the exponent in the empirical law [16,53]. However the luminosity functions of the Small Magellanic Cloud and M33 are not so well-behaved: compared to M31, these galaxies are a factor of ~ 2 deficient in PNe in the magnitude range $-2 < M_{5007} < +2$ [54,22]. Fortunately, this behavior (which depends on the system's star-formation history and is easily explained in terms of stellar evolution and photoionization theory) does not affect the bright end of the PNLF. It is therefore irrelevant for PNLF distance determinations.

Finally, before any distance can be derived, one must consider the effect of extinction on the distance indicator. For PNLF observations, the ratio of total to differential extinction is non-negligible ($A_{5007} = 3.5E(B - V)$ [55]), so this issue has some importance. There are two sources to consider: foreground extinction from the Milky Way, and internal extinction from the program galaxy. The former quantity is readily obtainable from reddening maps derived from H I measurements and galaxy counts [56] and/or from the DIRBE and IRAS satellite experiments [51]. However, the latter contribution to the total extinction is more problematic. In the Galaxy, the scale height of PNe is significantly larger than that of the dust [57]. If the same is true in other galaxies, then we would expect the bright end of the PNLF to always be dominated by objects in front of the dust layer. This conclusion seems to be supported by observational data [45,52] and numerical models [45], both of which suggest that the internal extinction which affects a galaxy's PN population is $\lesssim 0.05$ mag. We will, however, revisit this issue in Section 5.

4 Why the PNLF Works

The effectiveness of the PNLF technique has surprised many people. After all, a PN's [O III] $\lambda 5007$ flux is directly proportional to the luminosity of its central star, and this luminosity, in turn, is extremely sensitive to the central star's mass. Since the distribution of PN central star masses depends on stellar population via the initial mass-final mass relation [58], one would think that the PNLF cutoff would be population dependent.

Fortunately, this does not appear to be the case, and, in retrospect, the invariance is not difficult to explain. First, consider the question of metallicity. The [O III] $\lambda 5007$ flux of a bright planetary is proportional to its oxygen abundance, but since $\gtrsim 10\%$ of the central star's flux comes out in this one line, the ion is also the nebula's primary coolant. Consequently, if the abundance of oxygen is decreased, the nebula's electron temperature will increase, the number of collisional excitations per ion will increase, and the amount of emission per ion will increase. The result is that the flux in [O III] $\lambda 5007$ depends only on the square root of the nebula's oxygen abundance [15].

Meanwhile, the PN's core reacts to metallicity in the opposite manner. According to models of AGB and post-AGB evolution [59,60] if the metal abundance of a star is decreased, then the bound-free opacity within the star will decrease, and the emergent UV flux will increase. This will cause additional energy to be deposited into the nebula, and increase the amount of [O III] $\lambda 5007$ emission. Since this effect is small, and works in the opposite direction as the nebular dependence, the overall result is that the bright-end cutoff of the PNLF should be almost independent of metallicity.

A more sophisticated analysis by Dopita, Jacoby, & Vassiliadis [61] confirms this behavior. According to their models, the dependence of M^* on metallicity is weak and non-monotonic; a quadratic fit to the relation yields

$$\Delta M^* = 0.928[\text{O}/\text{H}]^2 + 0.225[\text{O}/\text{H}] + 0.014 \quad (3)$$

where [O/H] is the system's logarithmic oxygen abundance referenced to the solar value of $12 + \log(\text{O}/\text{H}) = 8.87$ [62]. Inspection of equation (3) reveals that M^* is brightest when the population's metallicity is near solar. In super-metal rich systems M^* fades, but since all metal-rich galaxies contain substantial populations of metal-poor stars, this part of the metallicity dependence should not be observed. Moreover, although M^* also fades in metal-poor systems, the change is gradual, so as long as the oxygen abundance of the host galaxy is $12 + \log(\text{O}/\text{H}) \gtrsim 8.3$ (*i.e.*, greater than two-thirds that of the LMC), the effect on distance determinations should be less than 10%. This weak dependence on metallicity is one reason why PNLF distances are so robust.

The reaction of the PNLF cutoff to population age is slightly less obvious, but no more complicated. Post-AGB evolutionary models [63,64] predict that the maximum luminosity and temperature achieved by a PN's central star is highly dependent on its core mass, with (very roughly) $L \propto M^3$ and $T_{\text{max}} \propto M^{2.5}$ for intermediate-mass hydrogen burning models. Consequently, high-mass central

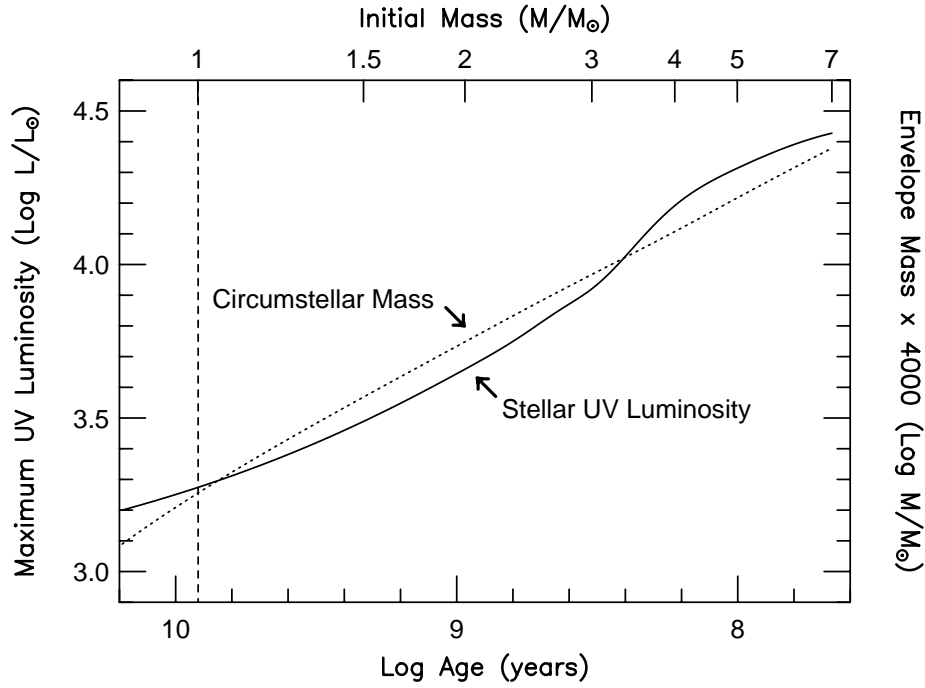


Fig. 4. A comparison of the maximum amount of ionizing radiation emitted by PN central stars against the mass of the stars' envelopes. The curves assume that the central stars are hydrogen burners [64] and use the Wiedemann initial-mass final-mass relation [58] with minimal RGB mass loss. The approximate lower-mass limit for PN progenitors is noted by a dotted line [66]; the conversion between initial mass and age comes from Iben and Laughlin [67]. The similarity of the relations implies that extinction will act to suppress the [O III] $\lambda 5007$ emission from high core-mass planetaries.

stars should be extremely bright in the UV and their nebulae should be exceptionally luminous in [O III] $\lambda 5007$. Since the mass of a central star is proportional to the mass of its progenitor (through the initial-mass final-mass relation [58]), this line of reasoning seems to imply the existence of some extremely luminous Population I planetaries. In fact, these over-luminous objects do exist. In the Magellanic Clouds, 9 out of the 74 planetaries with well-calibrated spectrophotometry [23,24,26] have intrinsic [O III] $\lambda 5007$ magnitudes brighter than M^* . Conversely, in the central regions of M31, where the bulge population dominates, only one out of 12 spectrophotometrically observed PNe is superluminous in [O III] [65]. However, *in every case*, these over-luminous objects are heavily extinguished by circumstellar material, so that no PN has an observed [O III] $\lambda 5007$ flux brighter than M^* .

In order to understand this phenomenon, one needs to consider the ratio of a nebula's input energy to its own circumstellar extinction. The former quantity is

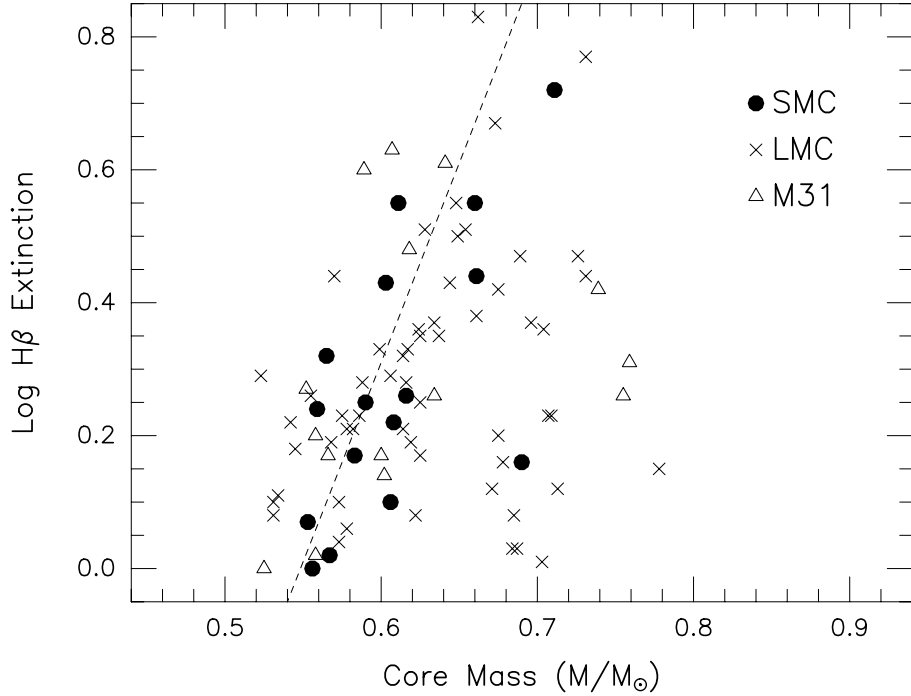


Fig. 5. The correlation between circumstellar extinction and central star mass for planetary nebulae in the Magellanic Clouds and M31. The extinction values are based on the Balmer decrement; the core masses have been derived via comparisons with hydrogen-burning evolutionary tracks. The slope of the relation is 5.7 ± 0.7 for the SMC, 6.3 ± 1.3 for the LMC, and 8.5 ± 1.6 for M31.

dictated by the central star's flux shortward of 912 \AA , which via the initial-mass final-mass relation, depends sensitively on the mass of the star's progenitor. The latter value is proportional to the amount of mass lost during the star's AGB phase, which is also set by the progenitor mass. Figure 4 compares these two values at the time when the central star's UV flux is greatest. Remarkably, the two functions are extremely similar throughout the entire range of progenitor masses. If the efficiency of circumstellar extinction is the same for all planetaries, then the figure implies that M^* will be independent of population age to within ~ 0.2 mag. Since self-extinction is probably more efficient around high-mass cores (since their faster evolutionary timescales give the material less time to disperse), this simple analysis suggests that high-mass PNe which are intrinsically more luminous than M^* will always be extinguished below the empirical PNLF cutoff.

Observational support for this scenario is shown in Fig. 5, which plots the relation between PN core mass and circumstellar extinction for [O III]-bright planetaries in the LMC, the SMC, and M31 [68]. The core masses of Fig. 5 have been derived by placing the central stars on the HR diagram (via photoioniza-

tion modeling of the PNe’s emission lines), and comparing their positions to the evolutionary tracks of hydrogen-burning post-AGB stars [64]; the plotted extinction estimates have been inferred from the PNe’s Balmer line ratios. Since the derived temperatures and luminosities of central stars have some uncertainty, and a fraction of PNe will be burning helium instead hydrogen, a good amount of scatter in the diagram is expected. Nevertheless, there is a statistically significant correlation between core mass and circumstellar extinction for the PN populations of all three galaxies. The best-fitting slope of $\sim 6 \text{ mag}/M_{\odot}$ more than compensates for the increased UV luminosity associated with the high-mass cores. In fact, when combined with the initial-mass final-mass relation [58], the steep slope of Figure 5 predicts that M^* should vary by less than $\sim 0.1 \text{ mag}$ in all populations older than 0.4 Gyr [68]. In younger populations, M^* may fade, but since all galaxies contain at least some stars older than $\sim 0.4 \text{ Gyr}$, this behavior should not be observable. The value of M^* in a star-forming galaxy should therefore be the same as that of an old stellar population.

5 Tests of the Technique

In the past decade, the PNLF has been subjected to a number of rigorous tests. In general, these tests fall into four categories.

5.1 Internal Tests Within Galaxies

The first and perhaps simplest test applied to the PNLF involves taking advantage of population differences within galaxies. Spiral galaxies have significant metallicity gradients [69], and the stellar population of a spiral’s bulge is certainly different from that of its disk and halo. Population differences exist in elliptical galaxies as well, as their radial color gradients attest [70]. If one can measure the distance to a sample of planetaries projected close to a galaxy’s nucleus, and then do the same for PN samples projected at intermediate and large galactocentric radii, one can determine just how sensitive the PNLF is to changes in stellar population.

Four galaxies now have large enough PN samples for this test: two Sb spirals (M31 [53] and M81 [71]), one large elliptical (NGC 4494 [72]), and one blue, interacting elliptical (NGC 5128 [44]). The data for M31 are shown in Fig. 6. No significant change in the PNLF cutoff has been observed in any of these objects. Given the diversity of stellar populations sampled, this result, in itself, is impressive proof of the robustness of the method.

5.2 Internal Tests within Clusters

A second internal test of the PNLF uses multiple galaxies within a common cluster. Galaxy groups are typically $\sim 1 \text{ Mpc}$ in diameter. PNLF distances to individual cluster members should therefore be consistent to within this value.

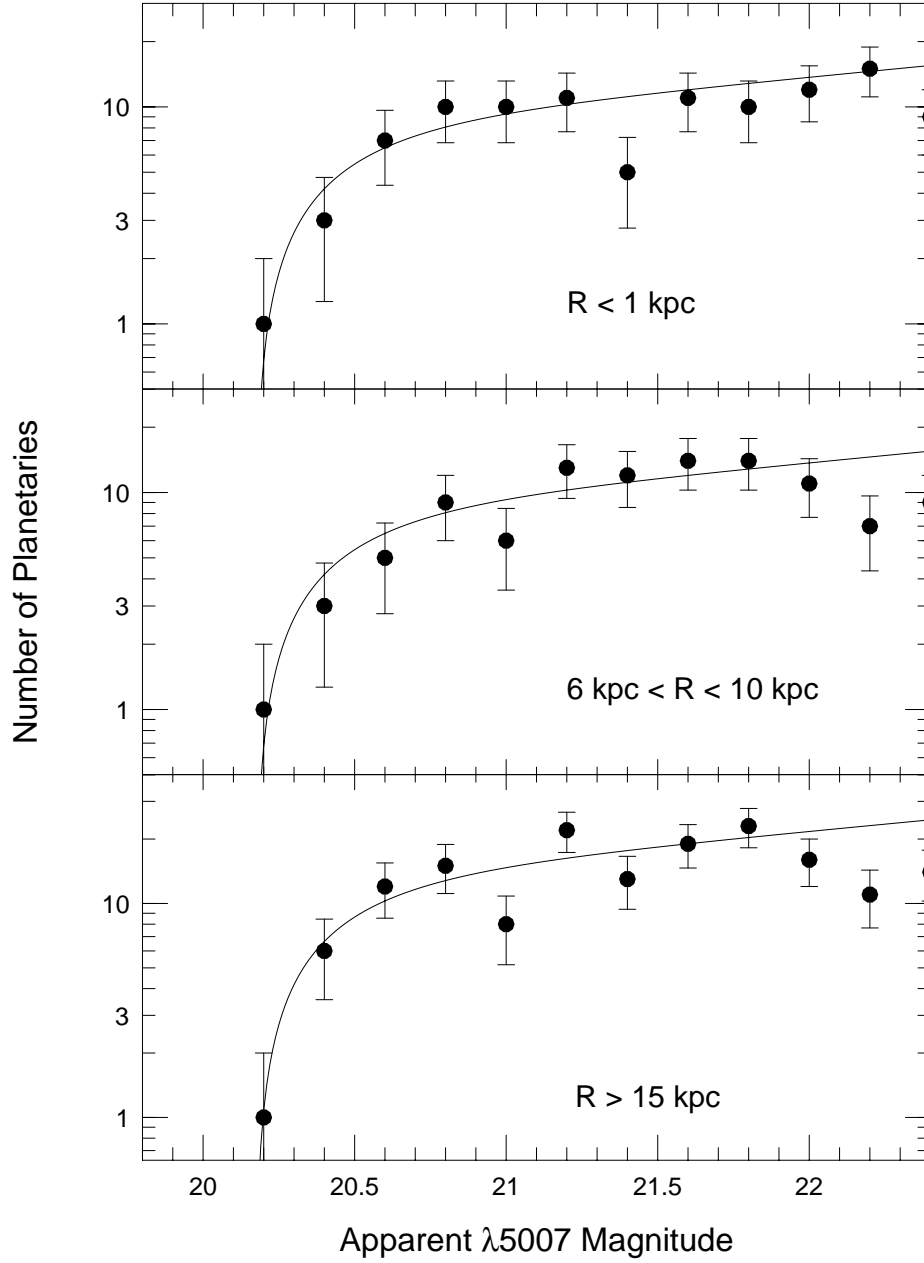


Fig. 6. The observed planetary nebula luminosity functions for samples of M31 PNe projected at three different galactocentric radii. The curves show the best-fitting empirical law. The derived PNLf distances are consistent to within ~ 0.05 mag. The turnover in the luminosity function past $m_{5007} \gtrsim 22$ in the intermediate and large-radius samples is real, and indicates the presence of relatively massive PN central stars.

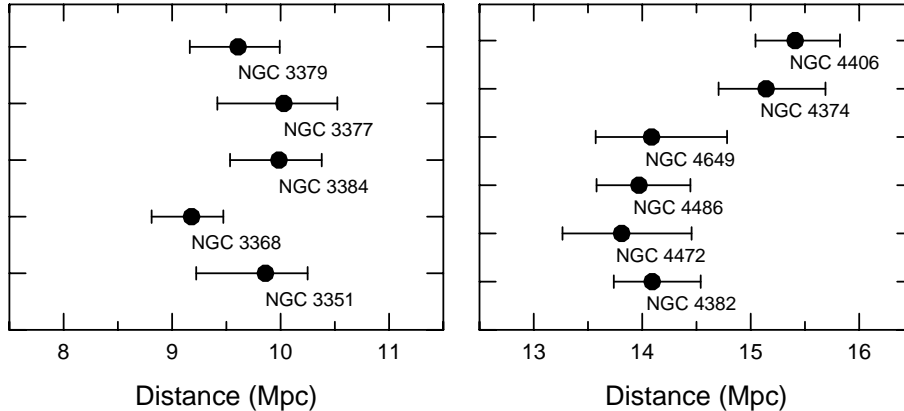


Fig. 7. PNLF distance measurements to the Leo I Group (left) and the Virgo Cluster (right). The Leo I galaxies possess a range of Hubble types from SBb to E0; the Virgo galaxies are all ellipticals or lenticulars, but range in color from $1.28 < (U - V) < 1.64$. The PNLF measurements in Leo I place all the galaxies within ~ 1 Mpc of each other, while in Virgo, the method easily resolves the background galaxies NGC 4374 and 4406 from the main body of the cluster.

Moreover, if the technique really is free of systematic errors, the measured distances should be uncorrelated with any galactic property, such as color, luminosity, metallicity, or Hubble type.

To date six galaxy clusters have multiple PNLF measurements: the M81 Group (M81 and NGC 2403 [17,45]), the NGC 1023 Group (NGC 891 and 1023 [73]), the NGC 5128 Group (NGC 5102, 5128, and 5253 [74,44,75]), the Fornax Cluster (NGC 1316, 1399, and 1404 [35]), the Leo I Group (NGC 3351, 3368, 3377, 3379, and 3384 [52,45,18]), and the Virgo Cluster (NGC 4374, 4382, 4406, 4472, 4486, and 4649 [37]). In each system, the observed galaxies have a range of color, absolute magnitude, and Hubble type. In none of the clusters is there any hint of a systematic trend. Indeed, as Fig. 7 indicates, PNLF measurements in Virgo easily resolve the M84/M86 Group, which is falling into the main body of Virgo from behind [76].

5.3 Comparisons with Cepheid Distances

Perhaps the most interesting test one can perform for any distance indicator is to compare its results to those of other methods. Such tests are crucial to the scientific method. While consistency checks, such as those described above, provide important information on the systematic behavior of a standard candle, external comparisons are the only way to assess the total uncertainty associated with a given rung of the distance ladder.

Figure 8 compares the PNLF distances of 13 galaxies (derived using the foreground extinction estimates from DIRBE/IRAS [51]) with the final Cepheid

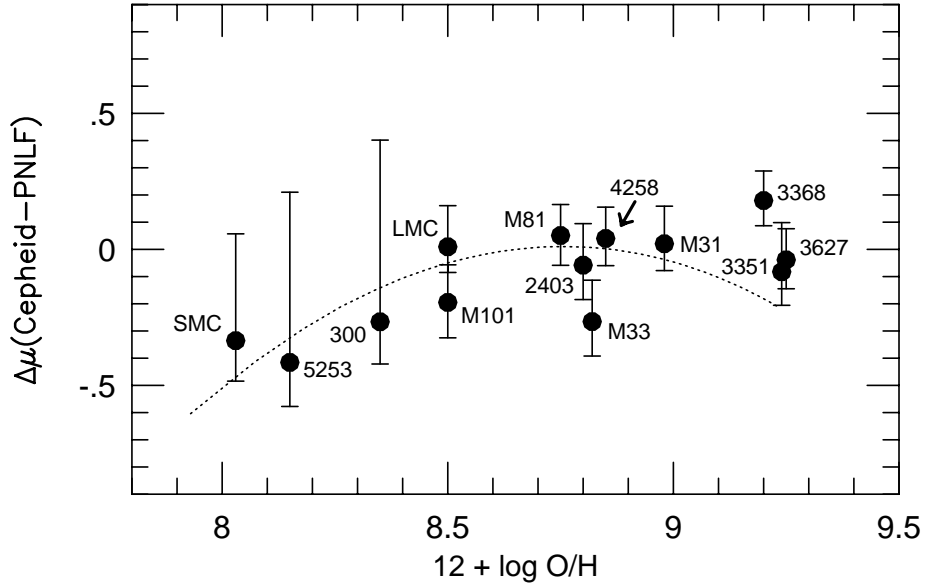


Fig. 8. A comparison of the PNLF and Cepheid distance moduli as function of galactic oxygen abundance, as estimated from the systems’ H II regions [77]. No metallicity correction has been applied to either distance indicator. The error bars represent the formal uncertainties of the methods added in quadrature; small galaxies with few PNe have generally larger errors. The curve shows the expected reaction of the PNLF to metallicity [61]. Note that metal-rich galaxies should not follow this relation, since these objects always contain enough low metallicity stars to populate the PNLF’s bright-end cutoff. The agreement between the two distance estimators is excellent, and the scatter is consistent with the internal errors of the methods.

distances produced by the *HST Key Project* [50]. Neither set of numbers has been corrected for the effects of metallicity. Since the absolute magnitude of the PNLF cutoff, M^* , is based on these Cepheid distances, the weighted mean of the distribution must, by definition, be zero. However, the residuals about this mean, and the systematic trends in the data, are valid indicators of the accuracy of the measurements.

As Fig. 8 illustrates, the scatter between the Cepheid distances and the PNLF distances is impressively small. Except for the most metal-poor systems, the residuals are perfectly consistent with the internal uncertainties of the methods. Moreover, the systematic shift seen at low-metallicity is exactly that predicted by PNLF theory [61]. If M^* were to be corrected using equation (3), the systematic error would completely disappear. This excellent agreement strongly suggests that neither the PNLF nor the Cepheid measurements need further metallicity corrections.

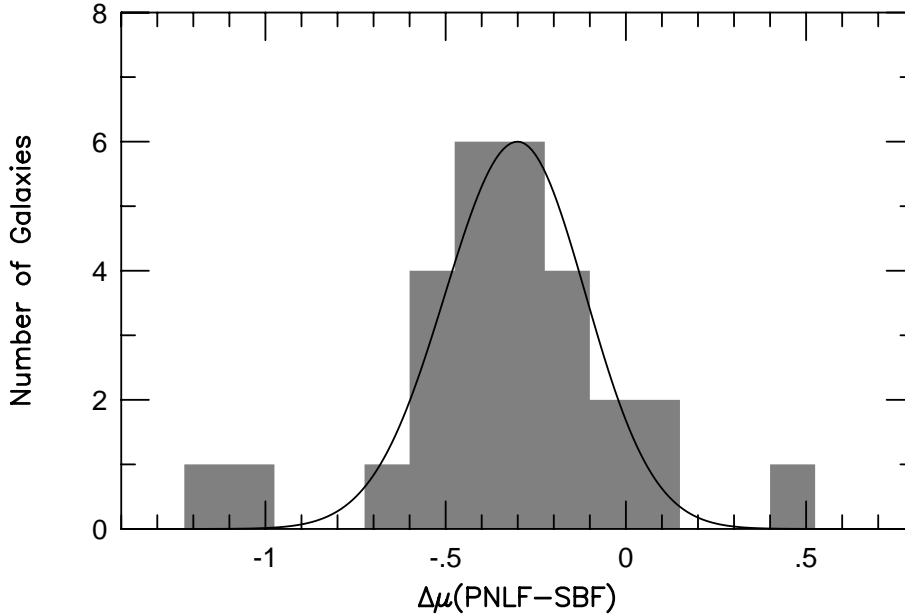


Fig. 9. A histogram of the difference between the PNLF and SBF distance moduli for 28 galaxies measured by both methods. The two worst outliers are the edge-on galaxies NGC 4565 ($\Delta\mu = -0.80$) and NGC 891 ($\Delta\mu = +0.71$). NGC 4278 is also an outlier ($\Delta\mu = -0.70$). The curve represents the expected dispersion of the data. The figure demonstrates that the absolute scales of the two techniques are discrepant, but the internal and external errors of the methods agree.

5.4 Comparisons with Surface Brightness Fluctuations

Another instructive comparison involves distances derived from the measurement of Surface Brightness Fluctuations (SBF) [36]. SBF distances have a precision comparable to that of the PNLF, but the technique can only be applied to smooth stellar populations, such as those found in elliptical and lenticular galaxies. Like the PNLF, SBF distances rely on Cepheid measurements for their calibration; consequently, a comparison of the two indicators gives a true measure of the external error associated with climbing a rung of the distance ladder.

To date, 28 galaxies have been measured with both the PNLF and SBF methods. A histogram of the distance residuals is shown in Figure 9. There are three important features to note.

The first interesting property displayed in the figure is the presence of three obvious outliers. The two worst offenders are NGC 4565 (-0.8 mag from the mean) and NGC 891 ($+0.7$ mag from the mean). Both are edge-on spirals — the only two edge-on spirals in the sample. Clearly one (or both) methods have trouble measuring the distances to such objects. Given the sensitivity of SBF

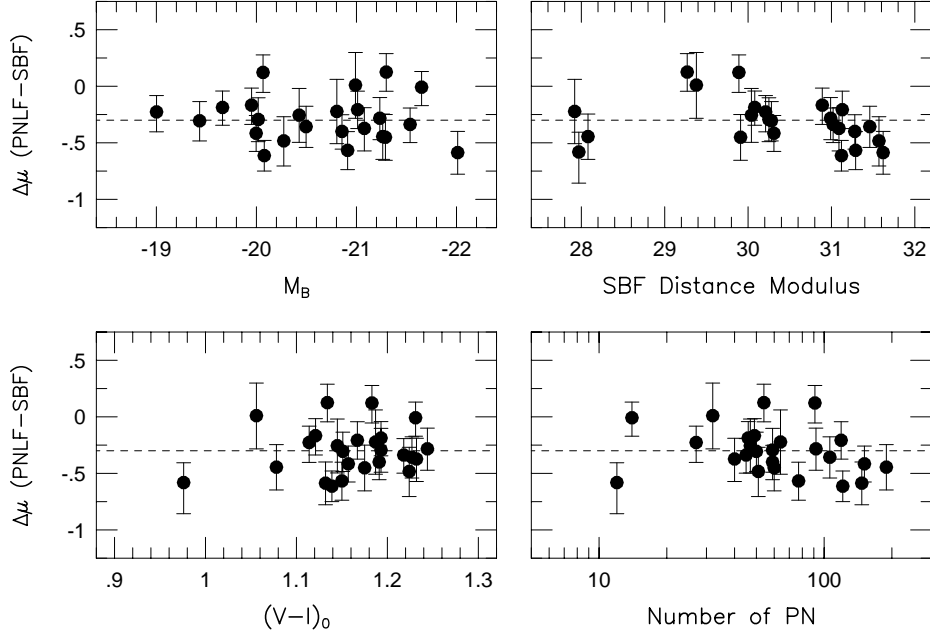


Fig. 10. The difference between SBF and PNLF distance moduli plotted against galactic absolute magnitude, distance, color, and number of PNe in the statistical sample. The three discrepant galaxies, NGC 891, 4565, and 4278, have not been plotted. The correlation with SBF distance modulus is marginally significant ($P \sim 0.1$), due to the low values of the five most distant objects; if these galaxies are removed from the sample, the significance of the correlation disappears. No other correlations exist in any of the panels.

measurements to color gradients, it is likely that the problem with these galaxies lies there, but an error in the PNLF technique cannot be ruled out.

The second important feature of Fig. 9 involves the scatter between the PNLF and SBF distance estimates. The curve plotted in the figure is not a fit to the data: it is instead the *expected* scatter in the measurements, as determined by propagating the uncertainties associated with the PNLF distances, the SBF distances, and Galactic reddening. It is obvious that the derived curve is in excellent agreement with the data. This proves that the quoted uncertainties in the methods are reasonable. It also leaves little room for additional random errors associated with measurements.

The latter conclusion is confirmed in Fig. 10. If either method were significantly affected by population age or metallicity, or if the PNLF fitting-technique were incorrect, then the PNLF-SBF distance residuals would correlate with galactic absolute magnitude, color, or PN population. No such trend exists. In fact, the only possible correlation present in the figure is with distance: if one *only* considers galaxies with $(m - M)_{\text{SBF}} > 30.6$, then the residuals do corre-

late with distance at the 95% confidence level. Such behavior might be expected if the PN samples found in distant galaxies were contaminated by background emission-line galaxies (or in the case of rich clusters, foreground intracluster stars). However, if the five most distant objects are deleted from the sample, the correlation goes away, proving that, in terms of relative distances, the PNLf and SBF techniques are in excellent agreement.

Interestingly, the same cannot be said for the methods' absolute distances. The PNLf zero point comes from planetary nebula observations in the 13 Cepheid galaxies displayed in Fig. 8; the formal uncertainty in M^* is ~ 0.05 mag. Similarly, the SBF zero point is based on fluctuation measurements in the bulges of six Cepheid spirals; its estimated uncertainty is ~ 0.04 mag. If both calibrations were accurate, then the mean of the PNLf-SBF distance residuals would be 0.0 ± 0.07 . It is not: as Figs. 9 and 10 indicate, SBF distances are, on average 0.30 ± 0.05 mag larger than PNLf distances. Even if the five most distant galaxies are excluded, the remaining ~ 0.26 mag offset is more than 3σ larger than expected. Clearly, there is an important source of error that is not being considered by one (or both) techniques.

The most likely explanation for the discrepancy involves internal extinction in the Cepheid calibration galaxies. To calibrate an extragalactic standard candle with Cepheids, one needs to measure the apparent brightness of the candle, m , and assume some value for the intervening extinction. Hence

$$M = m - \mu_{Cep} - R_\lambda E(B - V) \quad (4)$$

where M is the derived absolute magnitude of the object and R_λ is the ratio of total to differential reddening at the wavelength of interest. For most methods (including the PNLf), if the reddening to a galaxy is underestimated, then the brightness of the standard candle is underestimated, and the distance scale implied by the observations is underestimated. However, in the case of the I -band SBF technique, the standard candle, \bar{M}_I has a strong color dependence, with $\bar{M}_I = C + 4.5(V - I)_0$ [36]. Consequently, the zero-point of the system, C , is defined through

$$C = \bar{m}_I - \mu_{Cep} - 4.5(V - I)_{\text{obs}} + (4.5 R_V - 5.5 R_I) E(B - V) \quad (5)$$

Because $R_V > R_I$, an underestimate of reddening results in an overestimate of the brightness of the standard candle, and a distance scale that is too large. Since the PNLf and SBF methods react in opposite directions to reddening, even a small amount of internal extinction in the bulges of the calibrating spirals can lead to a large discrepancy between the systems in the exact sense that is seen. Specifically, if only the SBF measurements are affected, then the technique's distance scale will be too large by $4.2 \sigma_{E(B-V)}$ [55]. Moreover, if both techniques are affected, then $\sigma_{\Delta\mu} = 7.7 \sigma_{E(B-V)}$. With such a large coefficient, it would take only a small amount of internal reddening, $E(B - V) \sim 0.04$ mag to explain the discrepancy seen in the figures.

If internal extinction really is responsible for the offset displayed in Fig. 9, then the zero points of both systems must be adjusted. These corrections will

propagate all the way up the distance ladder. For example, according to the *HST Key Project*, the SBF-based Hubble Constant is 69 ± 4 (random) ± 6 (systematic) $\text{km s}^{-1} \text{Mpc}^{-1}$ [50]. However, if we assume that the calibration galaxies are internally reddened by $E(B - V) \sim 0.04$, then the zero point of the SBF system fades by 0.17 mag, and the SBF Hubble Constant increases to $75 \text{ km s}^{-1} \text{Mpc}^{-1}$. This one correction is as large as the technique’s entire systematic error budget. Such an error could not have been found without the cross-check provided by PNLF measurements.

5.5 Comparisons with Measurements Outside the Distance Ladder

No technique is perfectly calibrated, so distance measurements based on secondary standard candles, such as the PNLF, cannot avoid a component of systematic uncertainty. However, there are two galaxies in the local universe with distance estimates that do not rely on the distance ladder. The first is NGC 4258, which has a resolved disk of cold gas orbiting its central black hole. The proper motions and radial accelerations of water masers associated with this gas have been detected and measured: the result is an unambiguous geometric distance to the galaxy of $7.2 \pm 0.3 \text{ Mpc}$ [78]. The second benchmark comes from the light echo of SN 1987A in the Large Magellanic Cloud. Although the geometry of the light echo is still somewhat controversial, the most detailed and complete analysis of the object to date gives a distance of $D < 47.2 \pm 0.1 \text{ kpc}$ [79]. In Table 1 we compare these values with the distances determined from the PNLF [52] and from the measurements of Cepheids [50].

Table 1. Benchmark Galaxy Distances

Method	LMC	NGC 4258	$\Delta\mu$ (mag)
Geometry	$< 18.37 \pm 0.04$	29.29 ± 0.09	10.92 ± 0.10
Cepheids	18.50	29.44 ± 0.07	10.94 ± 0.07
PNLF	18.47 ± 0.11	29.43 ± 0.09	10.96 ± 0.14

According to the table, the Cepheid and PNLF methods both overestimate the distance to NGC 4258 by $\sim 0.14 \text{ mag}$, *i.e.*, by $\sim 1.3\sigma$ and 1.0σ , respectively. In the absence of some systematic error affecting both methods, the probability of this happening is $\lesssim 5\%$. On the other hand, there is no disagreement concerning NGC 4258’s distance *relative to that of the LMC*: the Cepheids, PNLF, and geometric techniques all agree to within $\pm 2\%$! Such a small error is probably fortuitous, but it does suggest the presence of a systematic error in the entire extragalactic distance scale.

In fact, the *HST Key Project* distances are all based on an LMC distance modulus of $(m - M)_0 = 18.50$ [50], and, via the data of Fig. 8, the PNLF scale is tied to that of the Cepheids. If the zero point of the Cepheid scale were shifted

to $(m - M)_0 = 18.37$, then all the measurements would be in agreement. This consistency supports a shorter distance to the LMC, and argues for a 7% increase in the *HST* Key Project Hubble Constant to $77 \text{ km s}^{-1} \text{ Mpc}^{-1}$.

6 Future Directions

The planetary nebula luminosity function is an excellent standard candle for measuring extragalactic distances within $\sim 20 \text{ Mpc}$. PNLF measurements are precise, and, in terms of telescope time, much more efficient than variable star monitoring or OB star spectroscopy. However, the technique cannot be extended much farther. Extragalactic PNe are point sources and their photometry is sky noise limited. Hence to maintain a constant signal-to-noise ratio, exposure times must grow as the fourth power of distance. Since PNLF measurements in Virgo already require $\sim 4 \text{ hr}$ of 4-m class telescope time in $\sim 1''$ seeing, observations at distances larger than $\sim 25 \text{ Mpc}$ are prohibitively expensive. Improvements in seeing, telescope aperture, and instrumentation will help slightly, but the PNLF will never be competitive with techniques such as Surface Brightness Fluctuations or the Tully-Fisher relation.

On the other hand, PNLF observations are unlikely to disappear. There will always be some objects, such as NGC 4258, for which an additional, high-precision distance measurement is useful. However, most future PNLF studies are likely to be performed as by-products of other investigations. Planetary nebulae are powerful tools for the study of astrophysics and cosmology. In addition to being excellent standard candles, PNe are useful probes of stellar population, unique tracers of chemical evolution, and excellent test particles for stellar kinematics and dark matter studies. Moreover, photometry and spectroscopy of planetary nebulae is the best and perhaps only way to study the line-of-sight distribution and kinematics of intracluster stars. Our study of the evolutionary state of nearby galaxy clusters has always been hampered by the limited number of test particles available for study [80]. However, these systems have plenty of planetary nebulae – in the core of Virgo alone, $\gtrsim 15,000$ intracluster planetaries are within reach of today’s telescopes. Thus wide-field [O III] $\lambda 5007$ imaging and follow-up spectroscopy in clusters such as Virgo and Fornax will be common in the coming decade.

All these programs, from the study of chemical evolution to the analysis of cluster kinematics, begin with the identification and photometric measurement of planetary nebulae. PNLF distances will therefore continue to be measured in the local universe.

I would like to thank G. Jacoby, J. Feldmeier, and P. Durrell for their comments during the preparation of this paper. This work made use of the NASA Extragalactic Database and was supported in part by NSF grant AST 00-71238.

References

1. E. Hubble: *Ap. J.* **84**, 270 (1936)
2. K.G. Henize, B.E. Westerlund: *Ap. J.* **137**, 747 (1963)
3. P.W. Hodge: *Galaxies and Cosmology*. (McGraw-Hill, New York 1966)
4. H.C. Ford, D.C. Jenner: *Bull. A.A.S.* **10**, 665 (1978)
5. D.G. Lawrie, J.A. Graham: *Bull. A.A.S.* **15**, 907 (1983)
6. G.H. Jacoby, M.P. Lesser: *A. J.* **86**, 185 (1981)
7. L. Berman: *Lick Obs. Bull.* **18**, 57 (1937)
8. R. Minkowski: *Pub. Obs. Univ. Mich.* **10**, 25 (1951)
9. I.S. Shkolovski: *Astron. Zh.* **33**, 222 (1956)
10. J.H. Cahn, J.B. Kaler, L. Stanghellini: *Astr. Ap. Suppl.* **94**, 399 (1992)
11. G.C. Van de Steene, A.A. Zijlstra: *Astr. Ap.* **293**, 541 (1995)
12. C.Y. Zhang: *Ap. J. Suppl.* **98**, 659 (1995)
13. T. Bensby, I. Lundström: *Astr. Ap.* **374**, 599 (2001)
14. J.P. Phillips: *Ap. J. Suppl.* **139**, 199 (2002)
15. G.H. Jacoby: *Ap. J.* **339**, 39 (1989)
16. R. Ciardullo, G.H. Jacoby, H.C. Ford, J.D. Neill: *Ap. J.* **339**, 53 (1989)
17. G.H. Jacoby, R. Ciardullo, H.C. Ford, J. Booth: *Ap. J.* **344**, 704 (1989)
18. R. Ciardullo, G.H. Jacoby, H.C. Ford: *Ap. J.* **344**, 715 (1989)
19. R.H. Eather, D.L. Reasoner: *Appl. Optics* **8**, 227 (1969)
20. A. Acker, F. Ochsenbein, B. Stenholm, R. Tylenda, J. Marcout, C. Schohn: *Strasbourg-ESO Catalogue of Galactic Planetary Nebulae*. (European Southern Observatory, Munich, 1992)
21. P.A. Shaver, R.X. McGee, L.M. Newton, A.C. Danks, S.R. Pottasch: *M.N.R.A.S.* **204**, 53 (1983)
22. P.R. Durrell, R. Ciardullo, M.B. Laychak, G.H. Jacoby, J.J. Feldmeier: *Bull. A.A.S.* in press (2003)
23. S.J. Meatheringham, M.A. Dopita: *Ap. J. Suppl.* **75**, 407 (1991)
24. S.J. Meatheringham, M.A. Dopita: *Ap. J. Suppl.* **76**, 1085 (1991)
25. E. Vassiliadis, M.A. Dopita, D.H. Morgan, J.F. Bell: *Ap. J. Suppl.* **83**, 87 (1992)
26. G.H. Jacoby, A.R. Walker, R. Ciardullo: *Ap. J.* **365**, 471 (1990)
27. E.M. Hu, L.L. Cowie, R.G. McMahon: *Ap. J.* **504**, 622 (1998)
28. R.-P. Kudritzki, R.H. Méndez, J.J. Feldmeier, R. Ciardullo, G.H. Jacoby, K.C. Freeman, M. Arnaboldi, M. Capaccioli, O. Gerhard, H.C. Ford: *Ap. J.* **536**, 19 (2000)
29. K.C. Freeman, M. Arnaboldi, M. Capaccioli, R. Ciardullo, J. Feldmeier, H. Ford, O. Gerhard, R. Kudritzki, G. Jacoby, R.H. Méndez, R. Sharples: 'Intracluster Planetary Nebulae in the Virgo Cluster'. In: *Dynamics of Galaxies: From the Early Universe to the Present, ASP Conference 197*, ed. by F. Combes, G.A. Mamom, V. Charmandaris (Astronomical Society of the Pacific, San Francisco 2000) pp. 389-392
30. R. Ciardullo, J.J. Feldmeier, K. Krelove, G.H. Jacoby, C. Gronwall: *Ap. J.* **566**, 784 (2002)
31. P.R. Durrell, J.C. Mihos, J.J. Feldmeier, G.H. Jacoby, R. Ciardullo: *Ap. J.* in press (2003)
32. J.J. Feldmeier, R. Ciardullo, G.H. Jacoby: *Ap. J.* **503**, 109 (1998)
33. P.R. Durrell, R. Ciardullo, J.J. Feldmeier, G.H. Jacoby, S. Sigurdsson: *Ap. J.* **570**, 119 (2002)
34. K. Krelove, J. Feldmeier, R. Ciardullo, P.R. Durrell: *Bull. A.A.S.* **32**, 1580 (2000)

35. R. McMillan, R. Ciardullo, G.H. Jacoby: Ap. J. **416**, 62 (1993)
36. J.L. Tonry, A. Dressler, J.P. Blakeslee, E.A. Ajhar, A.B. Fletcher, G.A. Luppino, M.R. Metzger, C.B. Moore: Ap. J. **546**, 681 (2001)
37. G.H. Jacoby, R. Ciardullo, H.C. Ford: Ap. J. **356**, 332 (1990)
38. N. Yasuda, M. Fukugita, S. Okamura: Ap. J. Suppl. **108**, 417 (1997)
39. M.J. West, J.P. Blakeslee: Ap. J. **543**, L27 (2000)
40. M. Arnaboldi, J.A.L. Aguerri, N.R. Napolitano, O. Gerhard, K.C. Freeman, J. Feldmeier, M. Capaccioli, R.P. Kudritzki, R.H. Méndez: A. J. **123**, 760 (2002)
41. R. Ciardullo, G.H. Jacoby, J.J. Feldmeier, R.E. Bartlett: Ap. J. **492**, 62 (1998)
42. G.H. Jacoby, R.J. Quigley, J.L. Africano: Pub. A.S.P. **99**, 672 (1987)
43. R. Ciardullo, H.C. Ford, J.D. Neill, G.H. Jacoby, A.W. Shafter: Ap. J. **318**, 520 (1987)
44. X. Hui, H.C. Ford, R. Ciardullo, G.H. Jacoby: Ap. J. **414**, 463 (1993)
45. J.J. Feldmeier, R. Ciardullo, G.H. Jacoby: Ap. J. **479**, 231 (1997)
46. R.H. Méndez, R.P. Kudritzki, R. Ciardullo, G.H. Jacoby: Astr. Ap. **275**, 534 (1993)
47. S.R. Pottasch: Astr. Ap. **236**, 231 (1990)
48. D.L. Welch, C.W. McAlary, R.A. McLaren, B.F. Madore: Ap. J. **305**, 583 (1986)
49. R.D. McClure, R. Racine: A. J. **74**, 1000 (1969)
50. W.L. Freedman, B.F. Madore, B.K. Gibson, L. Ferrarese, D.D. Kelson, S. Sakai, J.R. Mould, R.C. Kennicutt, Jr., H.C. Ford, J.A. Graham, J.P. Huchra, S.M.G. Hughes, G.D. Illingworth, L.M. Macri, P.B. Stetson: Ap. J. **553**, 47 (2001)
51. D.J. Schlegel, D.P. Finkbeiner, M. Davis: Ap. J. **500**, 525 (1998)
52. R. Ciardullo, J.J. Feldmeier, G.H. Jacoby, R.K. de Naray, M.B. Laychak, P.R. Durrell: Ap. J. **577**, 31 (2002)
53. X. Hui, H. Ford, G. Jacoby: Bull.A.A.S. **26**, 938 (1994)
54. G.H. Jacoby, O. De Marco: A. J. **123**, 269 (2002)
55. J.A. Cardelli, G.C. Clayton, J.S. Mathis: Ap. J. **345**, 245 (1989)
56. D. Burstein, C. Heiles: Ap. J. Suppl. **54**, 33 (1984)
57. D. Mihalas, J. Binney: *Galactic Astronomy*. (W.H. Freeman, New York 1981)
58. V. Weidemann: Astr. Ap. **363**, 647 (2000)
59. J.C. Lattanzio: Ap. J. **311**, 708 (1986)
60. E. Brocato, F. Matteucci, I. Mazzitelli, A. Tornabé: Ap. J. **349**, 458 (1990)
61. M.A. Dopita, G.H. Jacoby, E. Vassiliadis: Ap. J. **389**, 27 (1992)
62. N. Grevesse, A. Noels, A.J. Sauval: 'Standard Abundances'. In: *Cosmic Abundances, ASP Conference 99*, ed. by S.S. Holt, G. Sonneborn (Astronomical Society of the Pacific, San Francisco 1996) pp. 117-126
63. E. Vassiliadis, P.R. Wood: Ap. J. Suppl. **92**, 125 (1994)
64. T. Blöcker: Astr. Ap. **299**, 755 (1995)
65. G.H. Jacoby, R. Ciardullo: Ap. J. **515**, 169 (1999)
66. G.H. Jacoby, J.A. Morse, L.K. Fullton, K.B. Kwitter, R.B.C. Henry: A. J. **114**, 2611 (1997)
67. I. Iben, Jr., G. Laughlin: Ap. J. **341**, 312 (1989)
68. R. Ciardullo, G.H. Jacoby: Ap. J. **515**, 191 (1999)
69. D. Zaritsky, R.C. Kennicutt, Jr., J.P. Huchra: Ap. J. **420**, 87 (1994)
70. R.F. Peletier, R.L. Davies, G.D. Illingworth, L.E. Davis, M. Cawson: A. J. **100**, 1091 (1990)
71. L. Magrini, M. Perinotto, R.L.M. Corradi, A. Mampaso: Astr. Ap. **379**, 90 (2001)
72. G.H. Jacoby, R. Ciardullo, W.E. Harris: Ap. J. **462**, 1 (1996)
73. R. Ciardullo, G.H. Jacoby, W.E. Harris: Ap. J. **383**, 487 (1991)
74. R. McMillan, R. Ciardullo, G.H. Jacoby: A. J. **108**, 1610 (1994)

75. M.M. Phillips, G.H. Jacoby, A.R. Walker, J.L. Tonry, R. Ciardullo: *Bull. A.A.S.* **24**, 749 (1992)
76. H. Böhringer, U.G. Briel, R.A. Schwarz, W. Voges, G. Hartner, J. Trümper: *Nature* **368**, 828 (1994)
77. L. Ferrarese, H.C. Ford, J. Huchra, R.C. Kennicutt, J.R. Mould, S. Sakai, W.L. Freedman, P.B. Stetson, B.F. Madore, B.K. Gibson, J.A. Graham, S.M. Hughes, G.D. Illingworth, D.D. Kelson, L. Macri, K. Sebo, N.A. Silbermann: *Ap. J. Suppl.* **128**, 431 (2000)
78. J.R. Herrnstein, J.M. Moran, L.J. Greenhill, P.J. Diamond, M. Inoue, N. Nakai, M. Miyoshi, C. Henkel, A. Riess: *Nature* **400**, 539 (1999)
79. A. Gould, O. Uza: *Ap. J.* **494**, 118 (1998)
80. B. Binggeli, G.A. Tammann, A. Sandage: *A.J.* **94**, 251 (1987)